Sustainable Marine Structures

https://journals.nasspublishing.com/index.php/sms

ARTICLE

Active Learning-Based Construction of a Hydrodynamics Database for Critical Reynolds Numbers and Its Application to Vortex-Induced Vibrations Predictions

Hao Liu [1,2] **,** ***Jiasong Wang*** [1,2,3] **,** ***Yigang Gong*** [1,2] **,** ***Zhongxu Tian*** [4] **,** ***Yuanjiang Chang*** [5*]

[1] *Department of Engineering Mechanics, School of Ocean and Civil Engineering, Shanghai Jiao Tong University, Shanghai 200240, China*

[2] *Ministry of Education (MOE) Key Laboratory of Hydrodynamics, Shanghai Jiao Tong University, Shanghai 200240, China*

[3] *Yazhou Bay Institute of Deepsea Science and Technology, Shanghai Jiao Tong University, Sanya 572024, China*

[4] *College of Engineering Science and Technology, Shanghai Ocean University, Shanghai 201306, China*

[5] *Centre for Offshore Engineering and Safety Technology, China University of Petroleum (East China), Qingdao 266580, China*

ABSTRACT

For the cross-flow vortex-induced vibration (VIV) response of marine risers, comprehensive research has been conducted within the subcritical Reynolds number range. Despite ongoing efforts toward full-scale marine riser deployment, the understanding of VIV dynamics in the critical Reynolds regime remains limited. This is mainly due to the scarcity of high-fidelity data capturing key flow phenomena in this regime, including laminar separation bubbles, turbulent reattachment, and the drag crisis. This study established a hydrodynamic database for the critical Reynolds number regime using a custom high-resolution algorithm platform for incompressible flow (HRAPIF), leveraging Bayesian deep active learning (BDAL) to drive computational fluid dynamics (CFD) simulations. BDAL efficiently sampled the target in parameter space and established hydrodynamics coefficients with fewer large eddy

*CORRESPONDING AUTHOR:

Yuanjiang Chang, Centre for Offshore Engineering and Safety Technology, China University of Petroleum (East China), Qingdao 266580, China; Email: changyj@upc.edu.cn

ARTICLE INFO

Received: 16 April 2026 | Revised: 25 May 2026 | Accepted: 1 June 2026 | Published Online: 17 June 2026

DOI: https://doi.org/10.36956/sms.v8i2.3258

CITATION

Liu, H., Wang, J., Gong, Y., et al., 2026. Active Learning-Based Construction of a Hydrodynamics Database for Critical Reynolds Numbers and Its Application to Vortex-Induced Vibrations Predictions. Sustainable Marine Structures. 8(2): 225–247. DOI: https://doi.org/10.36956/sms.v8i2.3258

simulation (LES) runs. This database was embedded in the in-house code DAVIV for rapid prediction of VIV. Validated against Chaplin's experimental data, the prediction accuracy of DAVIV is comparable to that of SHEAR7 at subcritical Reynolds numbers. For full-scale risers, DAVIV provides more balanced performance and avoids excessive amplitude prediction at the critical Reynolds number. The result from DAVIV has good consistency with high-fidelity CFD. Overall, this framework addresses the bottleneck in VIV prediction accuracy within the critical Reynolds number regime, and provides a practical and low-cost tool for marine engineering.

Keywords: Vortex Induced Vibration; Critical Reynolds Numbers; Computational Fluid Dynamics; Riser Response Prediction

1. Introduction

Vortex Induced Vibration (VIV) is a classic fluid-structure interaction phenomenon that occurs when fluid flows around an elastically mounted bluff body, such as a circular cylinder. The alternating vortex shedding behind the body induces periodic forces, which may lead to large amplitude when the vortex shedding frequency approaches the natural frequency of the structure [1, 2]. Such results have attracted widespread attention in the field of marine engineering. Slender structures such as risers, pipelines and mooring cables are susceptible to fatigue damage or even failure under the action of periodic forces [3, 4]. Over the past decades, comprehensive efforts have been devoted to understanding the mechanisms of VIV, particularly through experimental measurement and numerical simulations. Feng [5] and Khalak and Williamson [6] identified distinct amplitude response branches in elastically mounted circular cylinders: the initial, upper, and lower branches. Subsequent research by Jauvtis and Williamson [7] revealed that allowing two-degree-of-freedom (2DOF) motion of cylinder, enabling both in-line and cross-flow displacements, can lead to even larger cross-flow amplitudes. Moreover, their work introduced a new wake pattern known as the 2T mode. With the development of computers and numerical methods these years, high fidelity numerical methods such as large eddy simulation (LES) and direct numerical simulation (DNS) have been widely employed to solve the complex wake dynamics and to validate experimental result [8, 9]. Chen et al. [10] conducted a systematic study on the vortex-induced vibration of a 2DOF circular cylinder at Re = 500 using three-dimensional DNS. They revealed the dual-branch response, multiple morphological displacement trajectories, phase difference jumps, and the variation laws of the three-dimensionality of the wake with amplitude under the coupling effect of the wall boundary layer and the cylinder wake. Chopra and Mittal [11] used numerical simulation system to depict the three-dimensional separation structure of a low aspect ratio cylinder near the critical Reynolds number. They clarified how the laminar separation bubble triggers secondary vortices, alters the vortex shedding mode, and suppresses vortex street. Sahu et al. [12] conducted the systematic numerical study of VIV responses and vortex structures in the supercritical region (fully turbulent boundary layer) using finite element large eddy simulation. They also analyzed the strength of vortex shedding after the drag crisis, the lock-in frequency, and the changes in amplitude branches. These simulations can provide detailed result about vortex formation modes and the transitions between different response branches.

The experiment about oscillating cylinder can systematically separate and quantify the hydrodynamic coefficients with the controlling of the amplitude and frequency. This feature provides a comparable research method for studying the vortex-induced forces of bluff bodies. This comparison method is based on a key assumption, initially proposed by Bishop and Hassan [13], which states that the hydrodynamic force acting on a forced oscillating cylinder is the same as the force applied on a freely vibrating cylinder under the same amplitude and oscillation frequency. This hypothesis has been widely validated and is consistent with the self-sustained vibration mechanism inherent in VIV. Morse and Williamson [14] used forced vibration data to predict the free VIV response, and drew a high-resolution hydrodynamic map (amplitude-frequency plane). And they predicted the free vibration amplitude, mode switching, and hysteresis through energy balance. Sarpkaya [15] comprehensively reviewed the VIV experiments, theories and models before 1979. He evaluated the advantages and disadvantages of various semi-empirical models and hydrodynamic databases at that time. He pointed out that high Reynolds number and three-dimensional effects are the key challenges for future research.

Based on confirmed hypothesis above, several empirical VIV prediction models have been developed to solve the VIV response rapidly, such as SHEAR7 and VIVANA. All these tools rely on hydrodynamic coefficient databases that are obtained from the oscillating cylinder experiment within subcritical Reynolds number range [16, 17]. These databases have enabled the implementation of an efficient, non-iterative prediction method for riser VIV, thereby significantly reducing computational costs while maintaining accuracy within the subcritical range.

Although these subcritical databases have achieved great success, the research on VIV has become more complicated due to the strong dependence on the Reynolds number. When Reynolds number comes into critical Reynolds number ranges, the boundary layer of the cylinder surface will undergo a transition from laminar to turbulent condition. The transition will alter the flow separation characteristic and vorticity field, then change the hydrodynamic forces [18]. The transition of the boundary layer is the core behavior within the critical Reynolds number (250,000–500,000). The most remarkable characteristic during this Reynolds range is the formation of what we called laminar separation bubble (LSB). What contributes to the formation of LSB is the delayed separation and the turbulence reattachment. Due to these behaviors, the drag coefficient has a rapid drop; this phenomenon is known as the drag crisis [19, 20]. While VIV has been comprehensively studied in the subcritical Reynolds number regime [21, 22], the characteristics remain poorly understood within the critical and supercritical Reynolds number range. Several studies have shown that VIV behavior at the critical Reynolds number differs substantially from that in the subcritical regime. At critical Reynolds numbers, the classic Kármán vortex street becomes indistinct, amplitude-response branches change, and sensitivity to free-stream turbulence and surface roughness increases [23, 24]. Most of the full-scale marine risers operate across a broad Reynolds number range; they often operate in conditions ranging from subcritical to supercritical Reynolds numbers. In that case, the necessity of thorough understanding about VIV at the critical Reynolds number has arisen. It can help us to prevent fatigue and damage in practical marine engineering [25].

The researchers conducted overall research in the construction of the database. Traditional databases establish a hydrodynamic database distribution covering the entire space by traversing each parameter point during experiments, and the traditional semi-empirical models mainly obtain the low-fidelity data. Due to the development of machine learning over the years, the prediction effect has been further enhanced. Combined with machine learning, a continuous functional mapping of hydrodynamic coefficients was constructed using sparse experimental data, thereby achieving rapid VIV evaluation in a wider parameter space [26, 27].

The construction of the hydrodynamic database mainly relies on experimental data. However, the cost of fully establishing the database is rising as the scale and complexity of the data increase. At the same time, machine learning methods have demonstrated significant potential in other scientific and engineering fields. Zhao et al. [28] employed random process simulation and Monte Carlo simulation in their studies. They quantified the uncertainty in structural response and assessed failure risk. This method provides an important reference for reliability of the engineering structures. Zhang et al. [29] developed a data-driven method for predicting battery end-of-life status using a TabNet model with Bayesian optimization. This approach achieved high-precision end-of-life classification, significantly outperforming traditional models such as Random Forest and XGBoost. Ye et al. [30] used Shapley value analysis and reverse stepwise regression algorithm to select key features, and they constructed six machine learning models for comparison. Finally, CatBoost was selected as the optimal model.

Meanwhile, the integration of machine learning into complex system modeling has undergone an important paradigm shift. The trend moves from black-box regression to physics-inspired and uncertainty-aware frameworks. In power systems, researchers have successfully combined physics-inspired time-frequency feature extraction with lightweight neural networks to enhance classification reliability [31]. Similarly, the adoption of hybrid neural networks optimized by metaheuristic algorithms (such as Beluga Whale Optimization) has demonstrated superior performance in predicting critical thermal states of transformers [32]. These achievements show an acknowledgement: the cooperation between physical laws and learning-based models is essential for navigating high-dimensional, non-linear spaces. Furthermore, AI-powered protein structure prediction now relies on active exploration of biochemical foundations to solve practical folding problems [33]. The principles of climate adaptation and corporate resilience in the low-carbon economy also highlight the necessity of models that can autonomously adapt to dynamic environmental shifts [34].

Although previous approaches based on alternative methods placed more emphasis on global approximation accuracy, inspired by these interdisciplinary innovations, our framework adopts an active learning strategy that prioritizes the utilization of utility. This framework conducts uncertainty quantification to guide the sampling process. This enables intelligent selection of high-fidelity computational fluid dynamics data points only in the areas where the physical responses are most uncertain, thereby ensuring the robustness of the prediction results and minimizing the computational cost.

Machine learning and surrogate models have been widely used in the past to construct hydrodynamic databases. However, most of the databases established either through machine learning optimization or through exhaustive experiments are still limited to subcritical Reynolds numbers. Fan et al. [26] proposed active learning guided by Gaussian process regression, which was experimentally validated but restricted to subcritical low Reynolds numbers. Meanwhile, the Gaussian process regression model relies heavily on artificial prior assumptions, such as kernel function selection. It performs poorly on high-dimensional problems, making it difficult to scale. Shen et al. [19] established a high-Reynolds-number database, but their approach relies on passive parameter-scanning experiments. This would require massive computational resources and time for numerical calculations. The experiments can only capture macroscopic behavior, being unable to address small-scale flow and flow field evolution. And those experiments [35] cannot capture key flow characteristics and fine structure such as laminar separation bubbles, turbulent reattachment, and drag crises. It is also difficult to observe the fine structure of the flow field in high Reynolds number experiments.

In contrast, this study employed a high-fidelity computational fluid dynamics (CFD) method to systematically construct a hydrodynamics database for the critical Reynolds number. This database originated from CFD simulations driven by active learning. Based on Bayesian active deep learning, the active learning strategy guides the sequential sampling of the parameter space, including frequency ratio and oscillation amplitude, to efficiently generate a continuous function mapping of hydrodynamic coefficients within the critical Reynolds number range. Moreover, it can capture the unique real physical mechanisms of the critical regions that are missing in the subcritical database. And it can also be directly applied to the prediction of full-scale risers. The database has been integrated into the self-developed DAVIV program and has been verified under the critical Reynolds number on the full-scale flexible riser model of ”Deep Sea No. 1”.

In this paper, Section 1 introduces the research background of riser vortex-induced vibration and the limitations of existing subcritical hydrodynamic databases; Section 2 presents the numerical methodology and active learning-driven CFD framework for constructing the critical Reynolds number hydrodynamic database; Section 3 demonstrates the validation and comparative analysis of VIV prediction results between the modified DAVIV program, SHEAR7 and relevant experimental data; Section 4 draws a conclusion.

2. Numerical Method

Figure 1 presents schematic diagrams of the fluid-structure interactions: **Figure 1a** shows the single-degree-of-freedom forced vibration of a rigid cylinder used for database construction, and **Figure 1b** shows the three-dimensional flexible vertical riser used for subsequent VIV predictions. These configurations also form the basis for subsequent research and discussion.

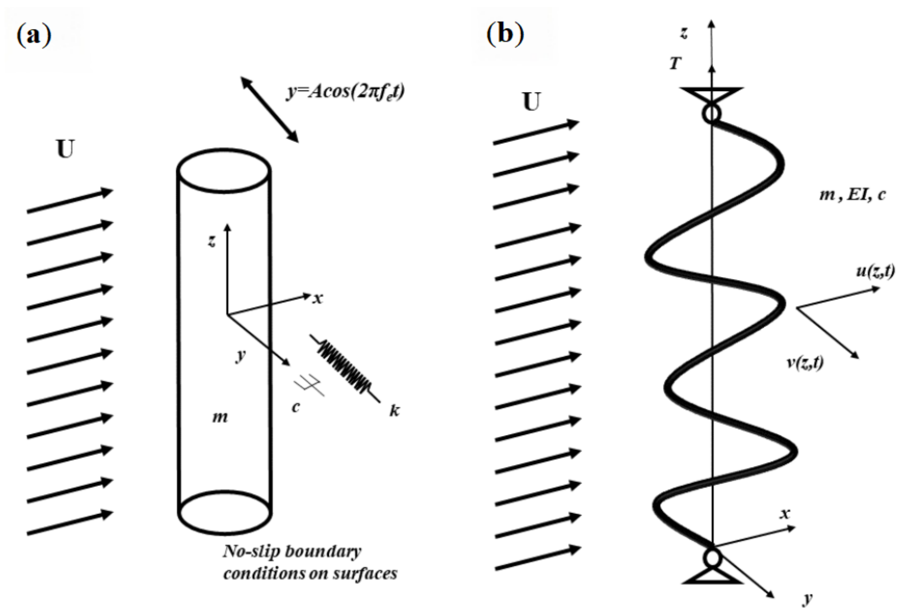

Figure 1. Schematic diagrams of rigid and flexible cylinders in fluid-structure interaction: (**a**) Single-degree-of-freedom rigid vibrating cylinder with a no-slip boundary condition applied to its surface; (**b**) Flexible riser with pinned-pinned ends under uniform inflow conditions.

2.1. Governing Equation

This study focuses on the vortex-induced vibration (VIV) of cylindrical structures subjected to ocean currents, with the fluid treated as incompressible and viscous. For transient incompressible flow, the continuity and Navier-Stokes equations can be written as:

$$\nabla \cdot u = 0 \tag{1}$$

$$\frac{\partial u}{\partial t} + u \cdot \nabla u = -\frac{1}{\rho}\nabla p + \nu \nabla^2 u \tag{2}$$

where u is the velocity vector, p is the pressure, ρ and ν are the fluid density and kinematic viscosity, respectively.

The structural response is modeled as a rigid cylinder undergoing a single-degree-of-freedom forced sinusoidal oscillation in the cross-flow (CF) direction. The cylinder displacement is given by:

$$y = A\cos(2\pi f_e t) \tag{3}$$

Where A is the oscillation amplitude and f_e is the oscillation frequency. To construct a high-fidelity hydrodynamic database, a large eddy simulation approach is employed to resolve the flow characteristics in the critical Reynolds number regime.

2.2. High-Fidelity Large Eddy Simulation (σ-LES)

A Reynolds number of 250,000 was selected because it marks the onset of the critical flow regime. Furthermore, several studies have been conducted within this range [36, 37]. The operating conditions of some full-scale risers in marine engineering often fall near this Reynolds number. Therefore, we believe setting it at 250,000 will help elucidate the detailed characteristics of the transition region.

For the critical Reynolds number (Re = 2.5×10^5), the σ-LES method is employed to resolve large-scale vortical structures. The spatially filtered continuity and momentum equations are:

$$\frac{\partial(\rho\widehat{u}_i)}{\partial t} + \frac{\partial(\rho\widehat{u}_i\widehat{u}_j)}{\partial x_j} = -\frac{\partial\widehat{p}}{\partial x_i} + \frac{\partial}{\partial x_j}\left[\mu\left(\frac{\partial\widehat{u}_i}{\partial x_j} + \frac{\partial\widehat{u}_j}{\partial x_i}\right)\right] - \frac{\partial\tau_{ij}^{SGS}}{\partial x_j} \tag{4}$$

where τ_{ij}^{SGS} is the subgrid-scale (SGS) stress tensor, which is closed using the σ-model. The SGS eddy viscosity is defined as:

$$\nu_{SGS} = (C_\sigma \Delta)^2 \frac{\sigma_3(\sigma_1 - \sigma_2)(\sigma_2 - \sigma_3)}{{\sigma_1}^2} \tag{5}$$

Here, $\sigma_1 \geq \sigma_2 \geq \sigma_3$ are the eigenvalues of the velocity gradient tensor $G = \widehat{g}^T \widehat{g}$, and Δ is the filter width. This turbulence model can accurately distinguish between laminar and turbulent regions. Consequently, σ-LES is well-suited for high-fidelity flow field simulations involving laminar separation bubbles (LSBs).

An O-type grid topology is used for the computational domain, with 25 spanwise layers, resulting in a total mesh count of approximately 4×10^6. The first-layer grid height near the wall satisfies y+ ≤ 1 to ensure adequate wall resolution. The computational domain spans 20D in width, 60D in length, and πD/2 in height. To clearly resolve the boundary layer, y+ is limited to less than 1 in this study. Furthermore, given the characteristics of vortex-induced vibration in the cylinder, mesh refinement is performed in both the inline and cross-flow directions. **Figure 2** shows a schematic diagram of the computational grid. The boundary conditions are illustrated in the current grid diagram: the upstream face of the cylinder is the inflow face, with inflow boundary conditions applied; the downstream face is the outflow face, with pressure outflow boundary conditions applied; the left and right sides of the cylinder are symmetrically distributed, with symmetric boundary conditions applied; and periodic boundary conditions are applied to the top and bottom of the cylinder.

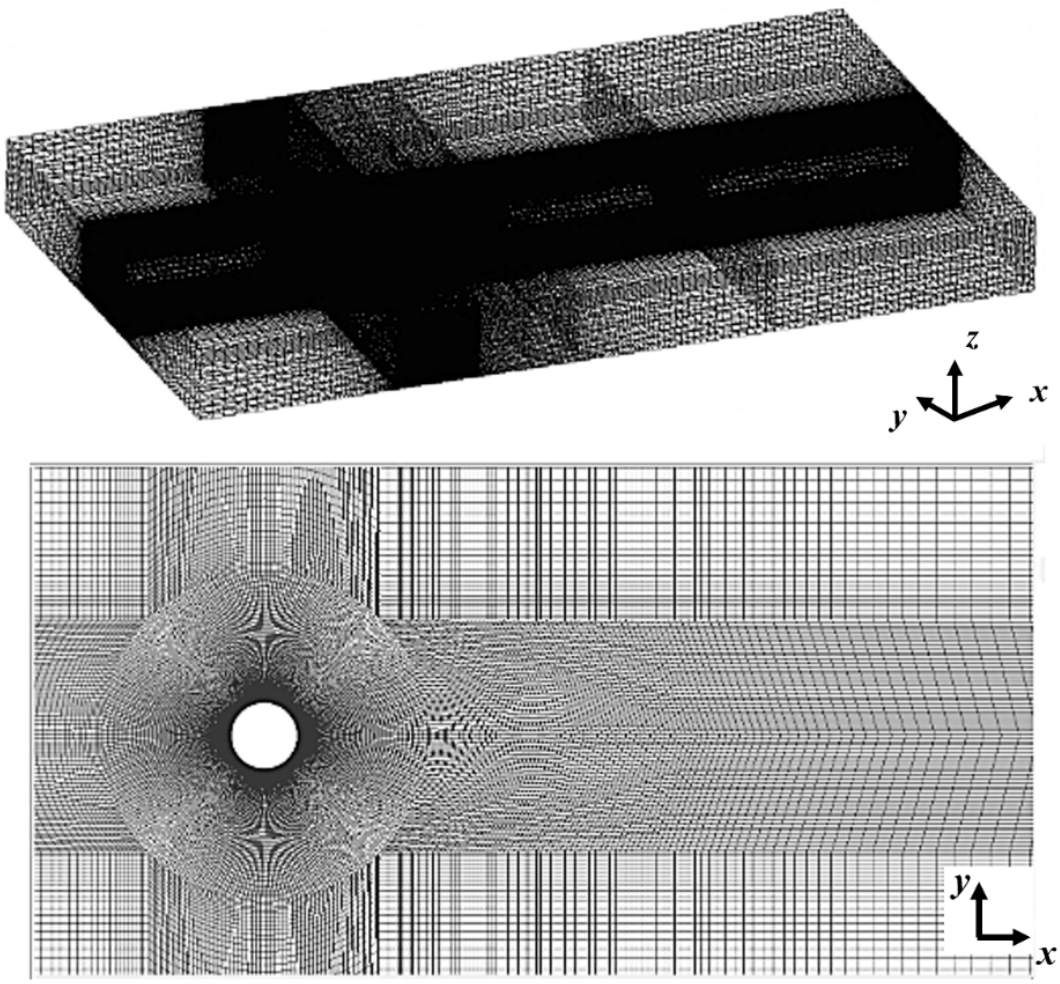

Figure 2. A multi-block structured grid, incorporating a near-wall boundary layer and grid refinement along two characteristic directions.

The inlet boundary is defined as a uniform velocity inlet, without introducing advanced turbulent fluctuation inflow techniques such as synthesized turbulent intensity profiles. For the Large Eddy Simulation (LES) computations, the maximum Courant-Friedrichs-Lewy (CFL) number is strictly maintained at 0.5. The temporal resolution is dynamically constrained and regulated by the solver based on the target CFL limit and the minimum cell height at the first grid layer.

Temporal derivatives are discretized using a second-order implicit scheme, which guarantees unconditional stability and relaxes the stringent constraints typically imposed by the CFL condition while preserving high temporal accuracy. For the convective terms, a central differencing scheme is blended with approximately 2% second-order upwind differencing. To preserve the stability of the implicit formulation, a deferred correction approach is implemented; the high-order convective scheme is partitioned into an implicit first-order upwind component and an explicit high-order correction source term. The viscous terms are discretized using the Gauss theorem and further decomposed into orthogonal and non-orthogonal correction components. Spatial gradients for all physical quantities are calculated using the least-squares method. Pressure-velocity coupling is achieved via the PIMPLE algorithm—a hybrid of the PISO and SIMPLE methods. The resulting pressure correction equations are solved using the stabilized biconjugate gradient (Bi-CGSTAB) method, accelerated by the BoomerAMG algebraic multigrid preconditioner. The entire numerical solver is integrated into the HRAPIF platform. Further details are shown in **Table 1**.

Table 1. Details of the CFD technology currently in use.

Parameter	Description
Mesh cases	48 divided Block-structured grid for MPI multi-CPU parallel computing. A refinement is implemented for the boundary layer and wake.
Grid size	The grid cells grow outward from the wall with a stretching ratio of 1.1. The cell number of each block is controlled to be approximately equal.
First-layer wall height (y+)	First-layer wall height is set to 10^{-4} m.
Time step & CFL setting	The CFL number in the entire computational domain is strictly controlled below 1.0.
Convergence criterion	Residuals at a single time step are less than 1×10^{-3}

It is noted that comprehensive grid independence verifications and time-step sensitivity analyses were rigorously conducted and verified in our previous studies; hence, they are omitted here to avoid redundancy.

2.3. Bayesian Neural Network-Driven Active Learning Framework

Given the high computational cost of three-dimensional LES and the scarcity of available data, it is crucial to identify sampling points with the highest information density to construct the hydrodynamic database. To address this issue, this paper employs a Bayesian deep active learning method to drive a three-dimensional LES program to perform active learning sampling, thereby automatically constructing a hydrodynamic database.

The core of this framework is to utilize the uncertainty quantification capability of the Bayesian model to guide high-information-content sampling. Ultimately, the database is constructed through interpolation based on the actual LES sampling points, rather than relying on the global predictions of the proxy model. The convergence criterion of the global prediction entropy reflects the completeness of information in the parameter space rather than the fitting accuracy of the proxy model.

A prior distribution $p(w)$ is assigned to the network weights, and variational inference is used to approximate the posterior distribution:

$$p(w \mid D) \approx q_\theta(w) \tag{6}$$

The network parameters are trained by maximizing the evidence lower bound (ELBO):

$$\mathcal{L}(\theta) = \mathbb{E}_{q_\theta(w)}\left[log_p(D|w)\right] - KL\left[q_\theta(w)||p(w)\right] \tag{7}$$

To capture heteroscedastic aleatoric noise, the network employs a dual-output architecture that predicts both the mean μ_{pred} and the log-variance $\log \sigma^2_{ale}$. During prediction, Monte Carlo sampling is used to compute the total uncertainty:

$$\sigma_{total} = \sqrt{\sigma^2_{epi} + \sigma^2_{ale}} \tag{8}$$

where σ_{total} is the epistemic uncertainty (model uncertainty) and σ_{ale} is the aleatoric uncertainty (data noise). Active learning uses predictive entropy as the acquisition function, combined with non-maximum suppression to avoid redundant sampling. This framework requires approximately 40 high-fidelity LES simulations to accurately capture the distributions of the excitation coefficient C_{lv}, added-mass coefficient C_{my}, and mean drag coefficient C_{dm}.

The efficiency improvement of active learning compared to traditional brute-force sampling is not simply a reduction in the number of samples, but stems from a change in the resource allocation logic. Assuming that all regions in the parameter space have the same value, it inevitably leads to resource mismatch and waste. This study's active learning follows the logic of information priority, precisely locates high-value regions through prediction uncertainty quantification, and fully allocates the limited computing resources to the areas where the impact on database accuracy is the greatest, while avoiding meaningless low-value calculations. Meanwhile, we do not perform uncertainty analysis on DAVIV prediction results.

2.4. Semi-Empirical Fast Prediction Method (DAVIV)

The dynamic characteristics of the riser structure are governed by several key factors: flexural rigidity, axial tension, and boundary conditions. The origin of the coordinate system is set at the sea level at the upper end of the riser. And the *z*-axis is vertically downward. The control equation for the motion can be expressed as follows:

$$\begin{aligned} &EI(z)\frac{\partial^4 u(z,t)}{\partial z^4} - \frac{\partial}{\partial z}\left(T(z)\frac{\partial u(z,t)}{\partial z}\right) \\ &+c(z)\frac{\partial u(z,t)}{\partial t} + m(z)\frac{\partial^2 u(z,t)}{\partial t^2} = f(z,t) \end{aligned} \tag{9}$$

In this equation, $u(z,t)$ is the riser's horizontal displacement, *EI* represents the flexural rigidity (product of the Young's modulus and the area moment of inertia), $c(z)$ is the hydrodynamic damping coefficient, *m* denotes the total linear density (including structural, internal flow, and added mass), and $f(z,t)$ is the distributed hydrodynamic force along the riser length.

To meet the need for rapid engineering predictions, this study employs the in-house semi-empirical VIV software DAVIV (Dynamic Analysis of Vortex Induced Vibration). This software is based on energy balance and modal superposition principles, and it discretizes the two-degree-of-freedom VIV control equation of the cylinder into a finite element form:

$$\mathbf{M}\ddot{q} + \mathbf{C}\dot{q} + \mathbf{K}q = \mathbf{F} \tag{10}$$

Here, **M**, **C**, and **K** are the mass, damping, and stiffness matrices, respectively, and **F** is the fluid excitation force vector. The fluid excitation force follows the Morison equation concept and is decomposed into a velocity-in-phase excitation term and an acceleration-in-phase added mass term:

$$F_y = \frac{\rho U^2 D}{2} C_{lv} cos\omega_l t \tag{11}$$

$$F_x = \frac{\rho U^2 D}{2} C_{dv} cos\omega_l t \tag{12}$$

where C_{lv} and C_{dv} are the excitation force coefficients in the CF and in-line (IL) directions, respectively. Traditionally, hydrodynamic data and models have been developed through forced vibration experiments, where the motion of a pipe section is prescribed to measure the resulting fluid forces. The derived lift and drag coefficients, along with the Strouhal number, are functions of the dimensionless amplitude, reduced velocity, and mass ratio. The widely used industrial software SHEAR7 can calculate the two-degree-of-freedom responses in both cross-flow direction and inline direction. However, it still uses the excitation force database under subcritical low Reynolds number conditions, and its prediction application scope is limited.

This study builds upon the original DAVIV program, which integrated the CF excitation database of Gopalkrishnan [38] (*Re* = 10,000) and the IL excitation database of Soni [39] (*Re* = 9,000) by extending the cross-flow database to the critical Reynolds number range. These databases are stored using a parameterization scheme similar to that of SHEAR7. In this study, we will use the original DAVIV program from the subcritical database to conduct a comparison of Chaplin's subcritical Reynolds number experiments. Additionally, predictions from the DAVIV program utilizing the critical Reynolds number database were compared against high-precision CFD results.

This solution method employs the modal superposition method, projecting the displacement $q(z,t)$ in the physical space onto modal coordinates $Q_k(t)$ as follows:

$$q(z,t)=\sum_k \phi_k(z)Q_k(t) \tag{13}$$

When calculating the response of each modal component, an iterative solution based on the energy balance principle is required. Specifically, the energy input and output sections for each mode must first be identified, a process that follows the method developed by Vandiver et al.[16] as described below. Based on the initial response amplitudes, the corresponding hydrodynamic forces are retrieved from a fluid force database. Subsequently, the energy input of the fluid force for the *k*th mode over a single cycle can be determined using Equation (14):

$$\Pi_k^{\mathrm{in}}=\int_{L_{\mathrm{in}}}\frac{1}{2}\rho DU^2(z)C_{lv}(z;\omega_k)A_k\omega_k\sin^2(\omega_k t)|\varphi_k(z)|\,dz \tag{14}$$

Here, C_{lv} is the hydrodynamic coefficient, A_k is the modal response amplitude, and L_{in} is the extent of the energy input region. The corresponding energy output for the *k*th mode is given by:

$$\Pi_k^{out}=\int_L R(z)\varphi_k^2(z)A_k^2\omega_k^2\sin^2(\omega_k t)dz \tag{15}$$

where $R(z)$ is the damping coefficient. The actual amplitude of the *k*th mode in the modal space is subsequently determined via energy balance considerations:

$$A_k=\frac{\frac{1}{2}\int_{L_{in}}C_{lv}(z;\omega_k)\,\rho\,DU^2(z)\,|\varphi_k(z)|\,dz}{\int_L R_s(z)\,\varphi_k^2(z)\,\omega_k\,dz+\int_{L-L_{in}}R_f(z)\,\varphi_k^2(z)\,\omega_k\,dz} \tag{16}$$

Once the updated amplitudes are obtained, the energy input and output are recalculated to proceed with the iterative solution. This process continues until the difference between two consecutive iterations converges to the fixed threshold. Consequently, a solution representing the fundamental energy balance of the riser's VIV is achieved.

3. Results and Discussion

Chaplin et al.[40, 41] conducted experiments in 2005 by comparing predictions from several semi-empirical engineering software tools of the time with their own measurements of VIV of a riser in a truncated uniform flow. The experiments were carried out in a water tank using a riser of length 13.12 m and diameter 0.028 m, with the lower 45% of its length exposed to a uniform flow and the upper part immersed in still water. To evaluate the predictive capability and accuracy of the DAVIV program for VIV responses, three representative cases from the experiments by Chaplin were selected. The detailed parameters and flow conditions, following the description by Huera-Huarte[42] regarding Chaplin experiments, are listed in **Tables 2** and **3**. Among these, Cases 2 and 3, which have relatively high top tensions, and Case 5, which has a low top tension and a low Reynolds number, were selected for validation. The results are presented in **Figure 3**, which shows the comparison among the experimental data, the DAVIV numerical simulation results, and the SHEAR7 prediction results[16] under different flow velocities.

Table 2. Structure parameters in the experiment by Chaplin.

Structural Parameter	Value
External diameter D (m)	0.028
Length (m)	13.12
Aspect ratio	470
Submerged length (m)	5.94
Bending stiffness EI (Nm^2)	29.88
Top tension (N)	350–2,000

Table 3. Different cases in experiment by Chaplin.

Case	**V (m/s)**	***Re***	**T_t (N)**
1	0.31	7,622	1,175
2	0.55	13,649	1,922
3	0.60	14,851	1,538
4	0.85	20,928	1,922
5	0.49	12,191	810
6	0.63	15,559	810
7	0.75	18,422	810
8	0.85	20,900	810

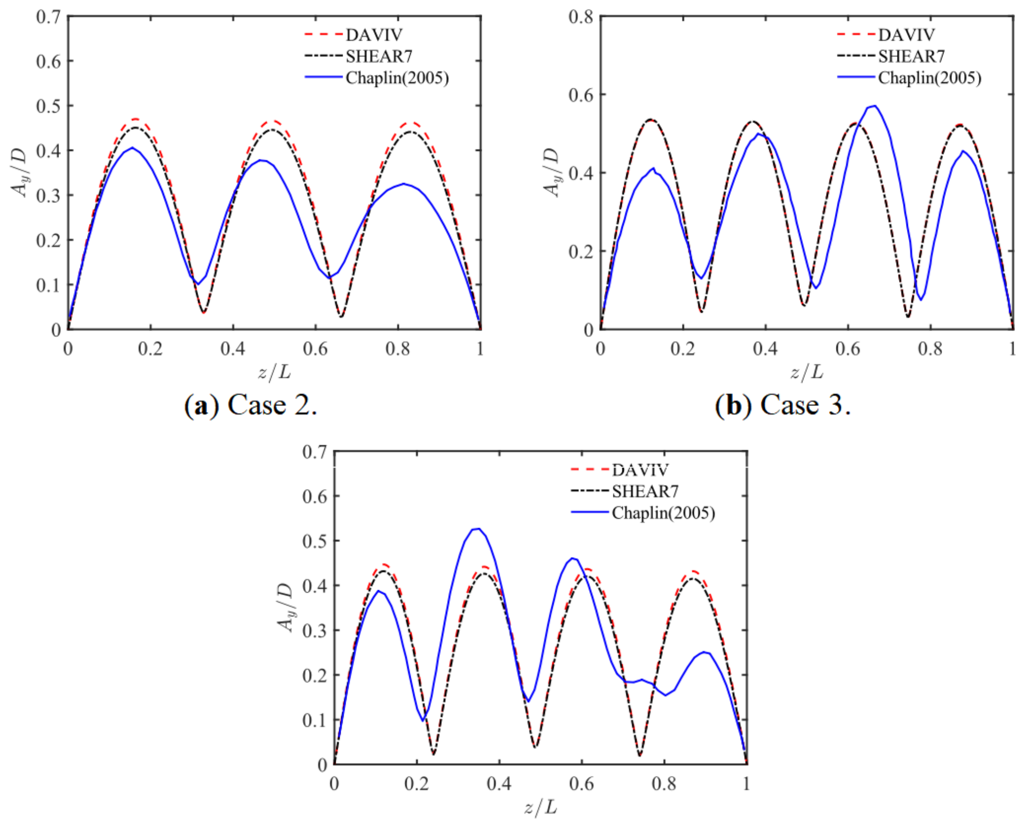

(**a**) Case 2. (**b**) Case 3. (**c**) Case 5.

Figure 3. Comparison of dimensionless cross-flow VIV displacement responses between the DAVIV, SHEAR7, and the Chaplin experimental data for three representative cases at subcritical Reynolds numbers.

Note: The cases correspond to different flow velocities and top tensions, as listed in **Tables 2** and **3**. Each subplot (**a**)–(**c**) shows the spanwise displacement envelope of the flexible riser.

The results in **Figure 3** showed that the predicted curves of DAVIV and SHEAR7 were highly overlapping. The RMSE differences between the two models were all less than 0.01, the MAPE differences were less than 1%, and the error improvement rate was within ±5%. This indicates that the two models have comparable predictive capabilities for the VIV amplitude distribution of the flexible riser. Compared with the experimental data, the errors of the two models under low-order modal conditions were smaller (MAPE ≈ 16%). As the modal order increased, the error slightly increased due to the asymmetric multi-peak characteristics of the experimental curve (MAPE ≈ 28%). Overall, they could still reflect the distribution trend of the vibration amplitude.

DAVIV effectively captured the modal characteristics of the riser VIV. The amplitude response of DAVIV was stable, and the predicted number of modes was consistent with the experimental results. Even as the experimental data exhibited more complex nonlinear characteristics at higher flow velocities, DAVIV maintained high prediction accuracy. The comparison of these three cases indicates that DAVIV has reliable calculation accuracy and wide applicability in predicting the VIV response of flexible risers. This program has comparable accuracy in predicting the VIV response of lateral flow to the semi-empirical software SHEAR7.

This study adopts the Bayesian deep active learning method, which is well suited for small-sample and high-Reynolds-number CFD simulation scenarios, to establish a dedicated hydrodynamic database for cylindrical VIV at critical Reynolds numbers. The database is obtained via high-fidelity three-dimensional large eddy simulation (LES) on the HRAPIF platform [43], targeting the typical critical Reynolds number condition $Re = 2.5 \times 10^5$ corresponding to the actual service environment of full-scale marine risers. The turbulence model and numerical method have been already introduced in present study [36]. Complete parametric hydrodynamic data collection and convergence analysis have been conducted for a rigid cylinder subjected to forced cross-flow oscillations, filling the research gap of scarce experimental and numerical data in this high critical Reynolds number regime, and providing reliable data support for the rapid prediction of VIV responses. The LES in this study was primarily conducted on a supercomputing platform. For the simulation of forced vibrations of a single-degree-of-freedom rigid cylinder under current critical Reynolds number conditions, the computational cost is influenced by the frequency ratio and amplitude ratio, with the frequency ratio having a particularly significant impact. The current computational mesh employs a multi-block structured grid divided into 48 grid blocks, thereby utilizing 48 cores simultaneously. The computational cost for a single high-fidelity LES case ranges from 4 days to 2 months, with total core-hours per operating condition ranging from 8,000 to 57,600. Based on approximately 40 LES calculations, the total computational cost for building the entire database is approximately 3 months.

This study generated 15 initial points in the parameter space defined by amplitude ratio and frequency ratio through random sampling, ensuring that the initial samples were uniformly and representatively distributed throughout the entire parameter domain, thereby avoiding local sampling redundancy or gaps. In each iteration, based on the prediction entropy criterion combined with the non-maximum suppression strategy, a fixed number of candidate samples were selected in batches for LES calculation, effectively avoiding the problem of sampling point aggregation within the parameter space. The iterative update was terminated when the global prediction uncertainty stabilized and the discrepancies between consecutive iterations were minimized. At this stage, the active learning loop shifted from global exploration to localized refinement, where introducing additional LES samples provided diminishing returns for database accuracy. In the preliminary study, the performance of different alternative models was compared. Considering the fluid dynamic characteristics under high Reynolds numbers discussed in this paper, the prediction entropy criterion was ultimately selected. This criterion provides a better balance between exploring unknown areas and identifying high-uncertainty areas, making it more suitable for constructing this hydrodynamic database.

The database we currently refer to only considers the two-dimensional parameter space distribution of amplitude ratio and frequency ratio, with a resolution of 0.025. The amplitude ratio ranges from 0.3 to 1.4, and the frequency ratio ranges from 0.4 to 1.6. The current range of forced vibration parameters is sufficient to cover the amplitude and frequency of vortex-induced vibration under critical Reynolds number conditions, and can be reasonably extrapolated under identical Reynolds number conditions, although parameters such as surface roughness are not yet included.

To evaluate the BDAL model's effectiveness in guiding the acquisition of key data points, we compared its distribution optimization performance against both random sampling and Latin hypercube sampling (LHS) across successive iterations, as illustrated in the **Figure 4a**. The Wasserstein distance was employed as the primary metric to quantify distribution discrepancies, where larger values indicate greater divergence. At the same time, **Figure 4b** shows the relationship between prediction accuracy and the number of iterations.

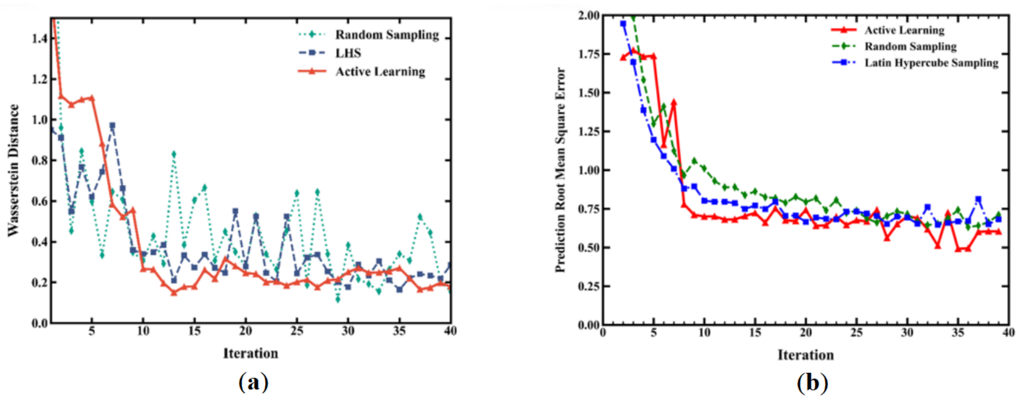

Figure 4. Evolution of (**a**) Wasserstein Distance and (**b**) RMSE Over Iterations: A Comparative Analysis of Random Sampling, Latin Hypercube Sampling (LHS), and the BDAL-Based Sampling Strategy for Critical Reynolds Number Database Construction.

The results demonstrate that the BDAL model consistently outperforms both baseline methods. Although the performance gap between LHS and BDAL narrows in the later stages, the samples captured by BDAL inherently possess higher information density—a critical advantage that blind sampling methods like LHS cannot replicate. Unlike conventional LHS, which fails to distinguish between data points of varying importance and often exhausts sampling capacity on redundant, low-value regions, BDAL intelligently prioritizes points that maximize the database's representational integrity.

Figure 5 illustrates the evolution of the database distribution patterns across the four distinct stages of the BDAL-driven sampling process. As shown by the distribution of selected sample points, the BDAL model not only ensures comprehensive coverage of the parameter space but also strategically prioritizes sampling density along the zero-contour line of C_{lv}. In regions characterized by high-gradient negative values, where gradients remain largely uniform and lack fine-scale features, the underlying distribution can be accurately reconstructed through simple linear interpolation. The BDAL model effectively identifies this behavior, thereby avoiding a common pitfall in active learning frameworks: the inefficient over-sampling of high-gradient zones that yields little to no improvement in global model accuracy.

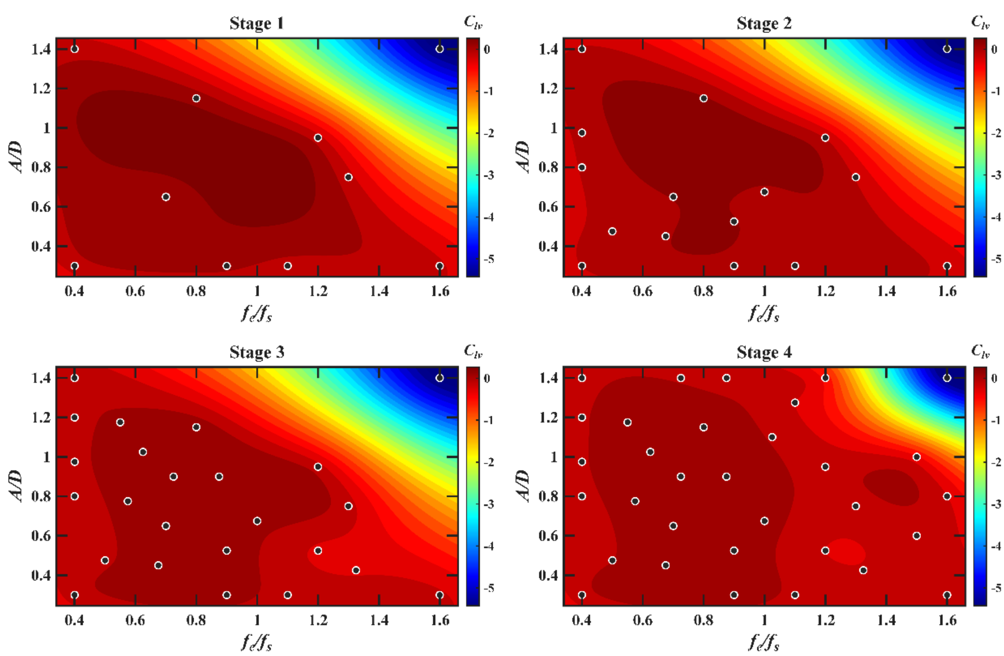

Figure 5. Evolution of the C_{lv} in the parameter space. Four-stage visualization of sampling points across the using BDAL-based sampling strategy.

Interpolation uncertainty is related to the spatial density of sampling points. In sparsely sampled regions, interpolation performance deteriorates due to insufficient effective constraint data, and the uncertainty introduced by interpolation cannot be ignored. However, based on current other experimental results, the distribution of the excitation force database differs from that of subcritical cases. The gradients in local distributions are very gentle with no abrupt changes. So it can be concluded that the accuracy of linear interpolation is acceptable. Furthermore, since the high-gradient negative-value regions are not actually used for VIV prediction, the resulting prediction errors are tolerable.

However, due to the limited number of samples, conventional interpolation tends to smooth out local features of the flow field to some extent and fails to capture sudden parameter changes; the resulting deviations become an additional source of error in DAVIV analysis. This issue can be addressed in future work by increasing the sampling density in low-density regions or by adopting more advanced interpolation algorithms.

As illustrated in the revised **Figure 6**, under the guidance of the BDAL model, the overall predictive entropy decreases monotonically across successive iterations. Crucially, the selection of each new sample point fundamentally reshapes the entropy landscape: once a point is sampled, its exact properties become fully deterministic, causing its local entropy to drop to zero. This localized information gain then propagates through the parameter space following the covariance structure (Gaussian kernel decay), thereby significantly suppressing the global epistemic uncertainty.

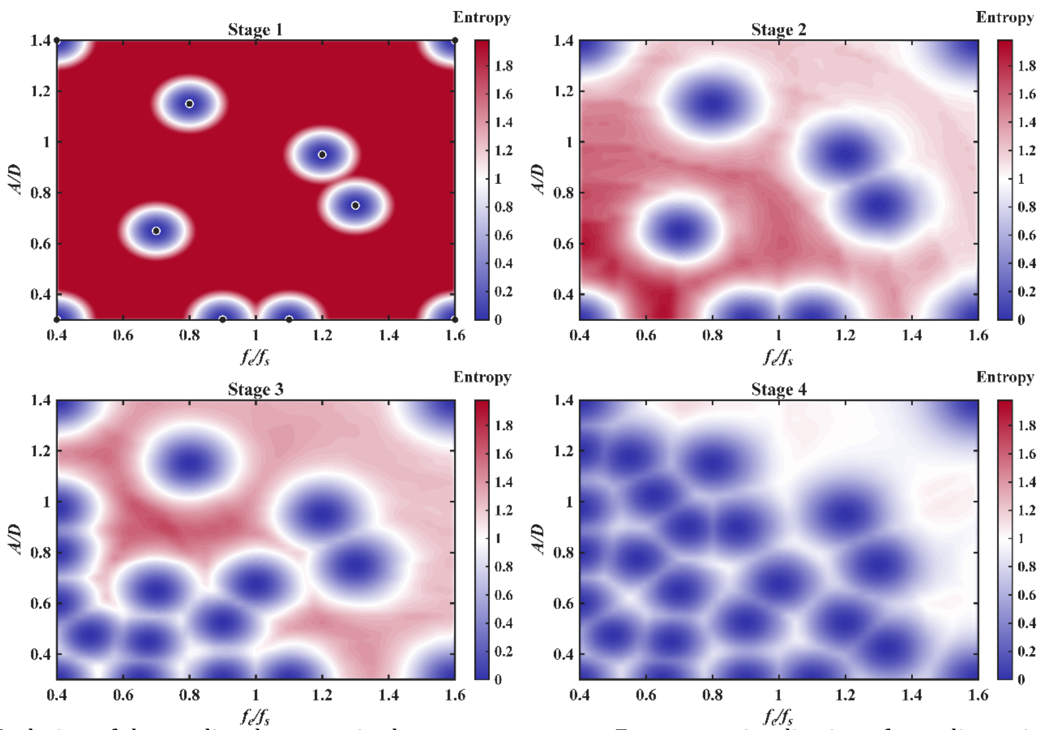

Figure 6. Evolution of the predicted entropy in the parameter space. Four-stage visualization of sampling points using the BDAL-based sampling strategy.

Therefore, we integrated the hydrodynamic coefficients derived from the 40 LES simulations into the DAVIV database to enhance the prediction of VIV responses at the critical Reynolds number. This database covers the complete distribution characteristics of three core hydrodynamic coefficients, namely the excitation coefficient C_{lv}, added mass coefficient C_{my}, and mean drag coefficient C_{dm}, within the two-parameter space of dimensionless frequency ratio f_e/f_s and amplitude ratio A/D, as shown in **Figure 7**. It clearly depicts the unique flow features of the critical flow regime distinct from subcritical and supercritical conditions, including the disappearance of the secondary amplification peak of the excitation coefficient, attenuation of non-resonant branches, drastic variation in the distribution pattern of the added mass coefficient, and the modulation effect of vibration parameters on the drag crisis around a cylindrical structure. These features fully reflect the coupling mechanism between boundary layer transition, wake vortex evolution and structural vibration at critical Reynolds numbers. Compared with conventional empirical databases at low Reynolds numbers, the database established in this study is more consistent with the actual flow conditions of full-scale marine engineering structures, and its data convergence and applicability have been numerically verified. It can be directly used as an accurate data source for the subsequent rapid prediction of marine riser VIV responses, parametric sensitivity analysis and response law judgment at critical Reynolds numbers, avoiding the repetitive implementation of time-consuming high-precision numerical simulations and effectively improving the efficiency of VIV prediction.

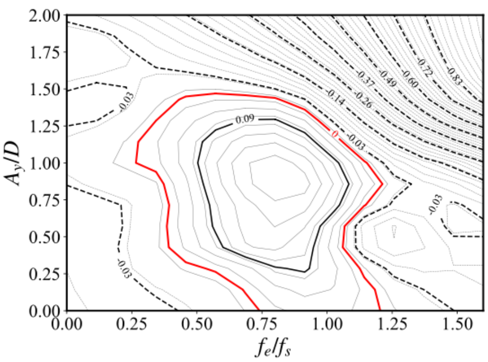

(a) C_{lv} distribution.

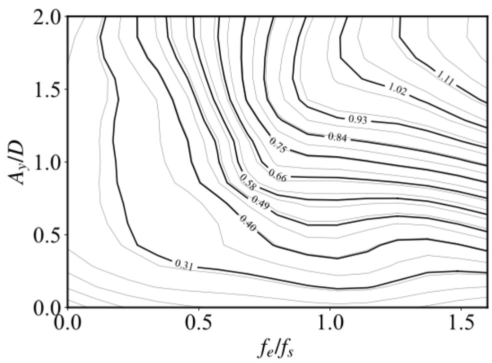

(b) C_{dm} distribution.

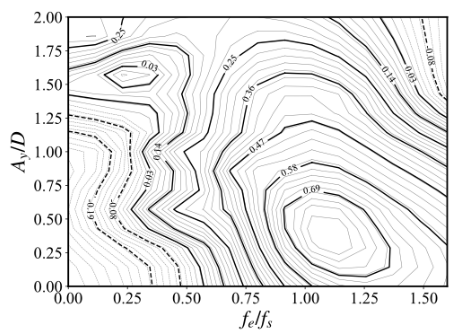

(c) C_{my} distribution.

Figure 7. Hydrodynamics coefficient database for a rigid oscillating cylinder at the critical Reynolds number (250,000). Subplots (**a**)–(**c**) show contour distributions of (**a**) the cross-flow excitation coefficient C_{lv}, (**b**) the mean drag coefficient C_{dm}, and (**c**) the added mass coefficient C_{my}, respectively. The coefficients are plotted as functions of the dimensionless amplitude ratio A_y/D and frequency ratio f_e/f_s.

This study does not aim to train a high-fidelity global surrogate model to fit the entire parameter space. Rather, the core approach is to use prediction uncertainty information to guide the sampling of real LES data in key high-information regions.

For sampling points where actual LES computations have been completed, the model simultaneously retains hydrodynamic coefficients along with their corresponding cognitive, aleatory, and total uncertainty information. For the remaining locations within the parameter space where LES sampling has not been conducted, a global hydrodynamic database is constructed using spatial interpolation based on existing real sampling points, rather than relying on point-by-point predictions from a surrogate model.

In the DAVIV vortex-induced vibration prediction framework, uncertainty is not propagated point-by-point using Bayesian networks; instead, calculations are performed directly using an interpolated hydrodynamic database for finite element hydrodynamic semi-empirical modeling.

Table 4 lists the structural parameters of the riser, which were tested at $Re = 2.5 \times 10^5$. These parameters correspond to full-scale operating conditions in the critical Reynolds number regime, where boundary-layer transition and drag crisis effects become prominent.

Figure 8 illustrates the axial distribution of the dimensionless cross-flow displacement amplitude along the flexible riser. This result is obtained using the DAVIV model updated with the proposed critical Reynolds number hydrodynamic database.

Table 4. Structural parameters of the riser which testing in $Re = 2.5 \times 10^5$.

Structural Parameter	Value
Length (m)	600
Inflow velocity (m/s)	0.5468
Line density (kg/m)	289.6
Bending stiffness EI (Nm^2)	1.07×10^8
Top tension (kN)	4,925

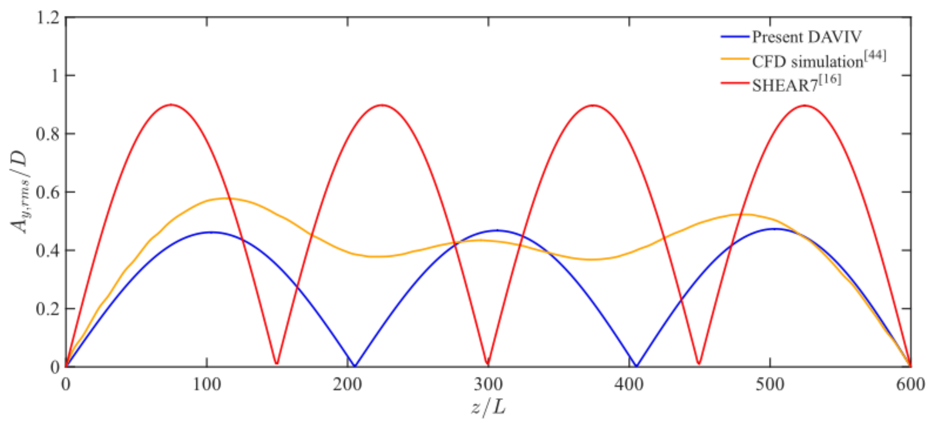

Figure 8. Cross-flow non-dimensional displacement predicted by DAVIV with the corrected database, in comparison with CFD simulation and SHEAR7 results (under critical Reynolds number $Re = 2.5 \times 10^5$).

Figure 8 also includes the CFD simulation results of Gong [44] and the prediction results of the conventional SHEAR7 program [16] for comparison. The present DAVIV prediction yields a relatively smooth amplitude distribution along the riser. CFD results show a similar modal distribution trend, indicating consistency in dominant-mode prediction between the two methods. On the other hand, the SHEAR7 solution relies on the conventional subcritical Reynolds number hydrodynamics database, which predicted considerable amplitudes and more obvious alternating peaks and valleys along the riser length. These differences highlight the influence of Reynolds-number effects on hydrodynamic loading and VIV responses.

SHEAR7 uses the hydrodynamic coefficients at subcritical Reynolds number, where laminar boundary layer separation and intense periodic vortex shedding are still present. This is the reason that results in enhanced excitation forces and thus overprediction of vibration amplitudes. In contrast, the DAVIV model updated with the present critical Reynolds number database accounts for boundary-layer transition, laminar separation bubbles, and the drag crisis typical of full-scale flow conditions, which suppress vortex shedding intensity and reduce hydrodynamic excitation.

Based on the CFD simulation results, a quantitative comparison was conducted on the lateral root mean square displacement distribution of the Present DAVIV and SHEAR7 models. The results showed that the RMSE and MAPE of Present DAVIV and CFD were 0.167 and 29.3% respectively. While the RMSE and MAPE of SHEAR7 and CFD were 0.321 and 62.1% respectively. Compared with SHEAR7, the error of Present DAVIV was reduced by approximately 48.0%, and the prediction accuracy was significantly improved. The direct comparison between the two models also indicated that the RMSE of DAVIV and SHEAR7 was 0.334, indicating that there were significant differences in the prediction of vibration amplitude distribution by the two models. The prediction results of DAVIV were closer to the CFD simulation.

As a result, the present DAVIV solution yields more moderate and physically consistent amplitude responses that align better with high-fidelity CFD results, demonstrating the importance of adopting Reynolds-number-dependent hydrodynamic databases for accurate VIV prediction of full-scale marine risers.

However, the agreement relies primarily on comparisons with CFD results rather than independent experimental evidence, which constitutes a specific limitation of the current work. Conducting experiments on full-scale risers hundreds of meters long under critical Reynolds number flow is extremely difficult. There are currently no reliable experimental data available for thorough validation. Future work should, where possible, include independent experiments or high-precision numerical results for cross-validation.

Table 5 lists the structural parameters of the full-scale flexible riser adopted from the “Deep Sea No. 1” platform [45], corresponding to the actual service conditions of deep-sea risers in the transitional Reynolds number regime.

Table 5. Structural parameters of the full-scale “Deep Sea No. 1” riser.

Structural Parameter	Value
Length (m)	300
Inflow velocity (m/s)	0.1–0.55
Line density (kg/m)	289.6
Bending stiffness EI (Nm^2)	1.07×10^8
Top tension (kN)	4,925

Figure 9 presents the three-dimensional axial distribution of dimensionless cross-flow displacement amplitude of the full-scale ”Deep Sea No. 1” riser, predicted by two methods: the modified DAVIV model with critical Reynolds number database and the widely-used engineering program SHEAR7. Both methods can capture the typical multi-modal vibration characteristics of the flexible slender riser, and the amplitude shows regular peak-valley alternation along the riser axial direction, precisely corresponding to the modal nodes and anti-nodes of each order of structural vibration modes, reflecting the inherent modal distribution law of fluid-structure interaction vibration of slender flexible structures. However, the dominant modal order differs between the two methods: SHEAR7 predicts a third-mode-dominated vibration, whereas the present DAVIV model yields a second-mode-dominated response.

In terms of amplitude magnitude and distribution pattern, the vibration amplitude predicted by SHEAR7 is generally higher, with the amplitude at anti-nodes approaching 0.9D, characterized by intense axial modal oscillation and an expanded fluctuation range. In contrast, the modified DAVIV model predicts a more stable response, with anti-node amplitudes remaining within 0.3D to 0.6D. Analyzed combined with the flow Reynolds number regime characteristics, the flow velocity in this study is in the transition regime from subcritical to critical Reynolds numbers, where the flow boundary layer evolution and vortex shedding characteristics are obviously different from those in the pure subcritical flow field. The built-in hydrodynamic coefficient database of SHEAR7 is obtained based on low-Reynolds-number subcritical flow tests, and its coefficient law is only suitable for the flow and vortex-induced excitation characteristics in subcritical flow fields, failing to adapt to the evolution of flow physical mechanisms in the transition regime, which is the core inducement of the response difference between the two methods.

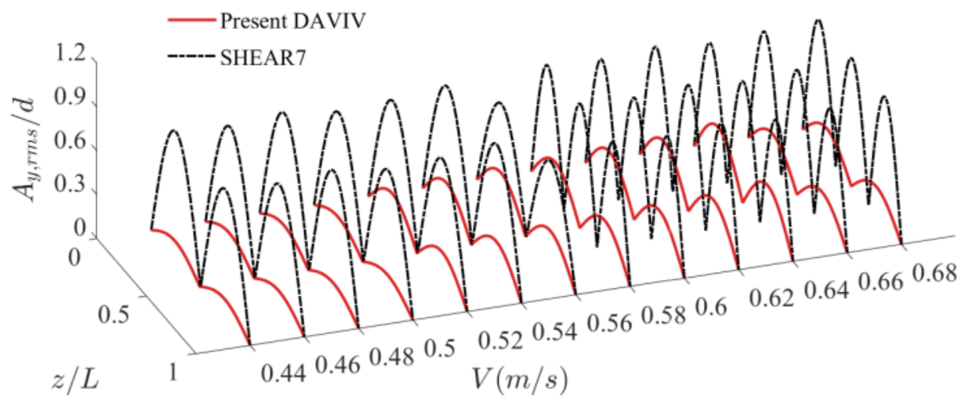

Figure 9. Cross-flow VIV amplitude distribution of the full-scale riser under varying inflow velocities: Comparison between the present DAVIV model (critical Reynolds number database) and SHEAR7.

Figure 10 further compares the maximum cross-flow vibration amplitude predicted by the two methods in the full velocity range. The present DAVIV program predicts a mean maximum amplitude of 0.198 across the entire velocity range, with a lower bound of 0.113 at 0.50 m/s and a peak response of 0.324 at 0.64 m/s. Conversely, SHEAR7 exhibits a highly conservative and severe overprediction, maintaining an elevated mean maximum amplitude of 0.852, which is 4.3 times higher than that of DAVIV. The maximum amplitude predicted by SHEAR7 reaches 0.892 at 0.54 m/s, overestimating the response by 63.7% compared to the peak value of DAVIV.

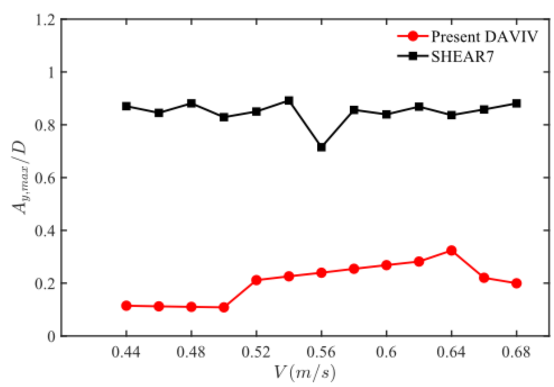

Figure 10. Comparison of maximum dimensionless cross-flow VIV amplitude between the present DAVIV model and SHEAR7 under varying inflow velocities.

Within the entire transition regime velocity range, the maximum amplitude predicted by SHEAR7 always maintains a high level of 0.7–0.9, with only a slight drop at 0.56 m/s, showing a consistently high-intensity vibration response without a clear amplitude evolution trend. In contrast, the modified DAVIV model predicts generally lower amplitudes, ranging from 0.1 to 0.33, and presents a clear trend of rising first, reaching the peak at 0.64 m/s and then slightly falling back. This variation law conforms to the real evolution logic of flow field-structural modal coupling in the transition regime: when the flow velocity further approaches the critical Reynolds number, the flow boundary layer characteristics gradually change, the vortex shedding excitation characteristics change, the coupling excitation energy cannot continue to increase, and the amplitude gradually decreases after reaching the peak. In contrast, the prediction results of SHEAR7 do not reflect the response changes caused by the flow field evolution in the transition regime.

Figure 11 shows the contour plot of absolute amplitude error predicted by the two methods, intuitively displaying the distribution characteristics of prediction differences along the riser axis and with flow velocity. In the low-velocity range where the flow field approaches subcritical (V < 0.56 m/s), high-error regions are concentrated at $z/L \approx 0.2$ and $z/L \approx 0.8$, which exactly correspond to the anti-nodes of the low-order vibration modes of the riser, while the errors at modal nodes and riser ends are extremely low, and the error distribution presents significant modal dependence. This is because the vibration amplitude at the modal anti-nodes is larger, and the adaptability difference of hydrodynamic coefficients is further amplified here.

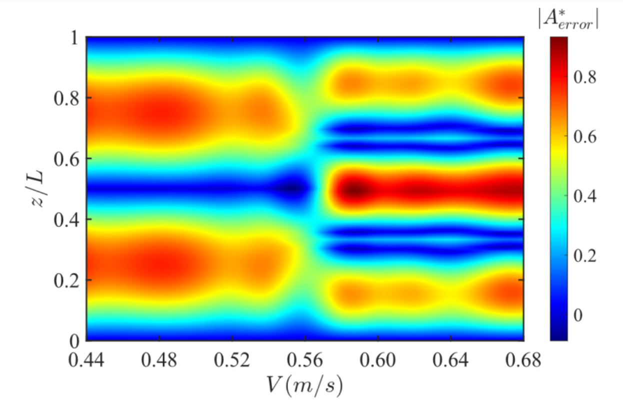

Figure 11. Contour of absolute VIV amplitude error for the riser at different uniform inflow velocities (comparison between the present DAVIV model and SHEAR7).

As the flow velocity increases and the flow field gradually deepens into the subcritical-critical transition regime, an obvious high-error band forms at the mid-span position $z/L\approx0.5$ of the riser, which is the anti-node region of higher-order modes and the region with the most significant evolution of flow field characteristics in the transition regime. Combined with the aforementioned amplitude distribution law, it can be seen that the prediction difference between the two methods is not caused by the numerical calculation method itself, but stems from the different working condition adaptation ranges of the hydrodynamic databases: the low-Reynolds-number subcritical database used by SHEAR7 does not match the current transition regime Reynolds number working conditions, and cannot fit the real physical mechanisms of flow field, fluid-structure interaction and structural modal vibration in this regime, eventually leading to systematic deviations in its prediction results under this working condition. This also confirms the necessity of adopting a hydrodynamic database suitable for high-Reynolds-number transition regime to improve the accuracy of vortex-induced vibration prediction for full-scale deep-sea risers.

Moreover, the discrepancy between the two predictions widens with increasing velocity, indicating that the limitations of subcritical hydrodynamic databases become more severe under conditions approaching the critical Reynolds number regime. This difference can be attributed to the differences in the flow physical mechanisms involved in the databases used by each method. The SHEAR7 program employs a hydrodynamic database at subcritical Reynolds number, where laminar boundary layer separation and periodic vortex shedding are more common. These phenomena lead to enhanced excitation forces and subsequent overestimation of the amplitude. In contrast, the current DAVIV model updates the critical Reynolds number database and considers boundary layer transition, laminar separation bubbles, and drag crises. All these considerations are key features of full-scale flow conditions at critical Reynolds number. These critical Reynolds number phenomena reduce the excitation effect of hydrodynamics, which generate a more moderate and more consistent amplitude response with the full-scale marine risers operating environment. By capturing the unique flow physical characteristics during the transition state of Reynolds numbers, the current method provides a more physically consistent and accurate assessment of VIV responses. These results emphasize that when operating full-scale marine structures in high Reynolds number environments, a Reynolds number-related hydrodynamic database must be adopted.

Although this study yields promising results for riser hydrodynamic response prediction, several inherent technical limitations must be acknowledged when extending these findings to full-scale deepwater engineering applications.

First, regarding the hydrodynamic inputs, this work adopts a simplified crossflow oscillating cylinder, thereby neglecting the highly coupled cross-flow and in-line orbital trajectories. This simplification fails to capture the vortex-shedding mode transitions induced by orbital motions in wakes, potentially leading to non-linear deviations in hydrodynamic coefficients within high-amplitude regimes. Concurrently, the idealized smooth-cylinder assumption overlooks the surface roughness effects generated by operational degradation on real-world risers. Such roughness can prematurely trigger boundary layer transition and significantly alter drag coefficients. Furthermore, the present simulations are conducted under uniform flows with no turbulence. In contrast, turbulence fluctuations in ocean currents tend to accelerate wake dissipation and disrupt the spanwise coherence of vortex shedding, ultimately leading to narrower lock-in bandwidths and attenuated peak amplitudes in field environments.

Second, regarding structural response dynamics in strongly sheared ocean currents, these flexible structures often exhibit alternating traveling and standing wave responses driven by complex multi-modal competition. The frequency-domain approach adopted herein inherently lacks the capability to fully resolve these transient, multi-modal time-history features.

Finally, concerning extrapolative robustness under extreme conditions, the parameter validation and database construction in this study are strictly concentrated within the critical Reynolds number regime. Marine risers routinely operate in supercritical or ultra-high Reynolds number regimes where the boundary layer becomes fully turbulent and vortex street restructuring may occur. Due to the lack of dedicated mechanisms within the present framework to capture turbulent transition and laminar separation bubble evolution at broader Reynolds numbers, direct extrapolation to such supercritical engineering conditions should be approached with caution.

All in all, this study proposes a BDAL-driven framework for hydrodynamic database construction and full-scale riser VIV prediction. While enhancing the capture accuracy of hydrodynamic characteristics within the critical Reynolds number regime, this methodology establishes a viable paradigm for practical deepwater engineering applications. In terms of workflow integration and cost-benefit alignment for engineering deployment, despite the current frequency-domain solver's limitations in capturing time-domain transient responses, the adaptively generated database serves as a high-fidelity data source that can be seamlessly integrated into existing industrial semi-empirical prediction programs (e.g., DAVIV). Regarding framework scalability, this active learning–database–semi-empirical prediction architecture exhibits algorithmic universality. Although the current database construction has some limitations, the underlying logic is inherently independent of specific flow regimes. Future research will retain this core algorithmic framework while introducing further physical refinements. This will further extend the framework to wider Reynolds number regimes, laying a technical foundation for constructing comprehensive full-scale hydrodynamic databases across the entire flow regime of marine risers.

4. Conclusion

This study utilized the Bayesian active learning method to drive the high-fidelity σ-LES simulations for sampling, and constructed a unique hydrodynamic coefficient database at a critical Reynolds number ($Re = 2.5 \times 10^5$). This database was integrated into the semi-empirical in-house DAVIV program so as to be able to accurately predict the VIV of full-scale risers. The main research results and conclusions are summarized as follows.

(1) When utilizing the subcritical hydrodynamic database, the DAVIV program achieves predictive accuracy comparable to the established engineering software SHEAR7, as validated against the Chaplin riser VIV experiments. It can capture modal features and amplitude envelopes, confirming the stability of the semi-empirical framework. Meanwhile, for full-scale deep-sea risers operating at critical Reynolds number, the present DAVIV program demonstrates more suitable response prediction compared to SHEAR7 when using hydrodynamics database at critical Reynolds number. The present DAVIV program has captured the effect of these flow features on the fluid excitation force, thereby generating an amplitude response that is more consistent with the highly accurate CFD results.

(2) The results under different flow velocity conditions indicate that the prediction error between DAVIV and SHEAR7 gradually increases as the flow transitions from subcritical to critical Reynolds number range. The subcritical Reynolds number database fails to capture the evolution mechanism during the transitional state, causing SHEAR7 to overestimate the amplitude of the VIV by up to 0.9D. This indicates that when predicting amplitude response of risers, the database that matches the operating Reynolds number conditions should be used.

(3) This study proposes an extensible methodology for vortex-induced vibration prediction. Through an active learning mechanism, it achieves a paradigm shift from the blind, exhaustive logic of orthogonal experiments to active, optimal information acquisition. Furthermore, the validity of the current database has been verified through comparison with high-precision CFD results. This framework provides a more robust decision-making basis for selecting engineering solutions, offering significant scientific exploration value and engineering guidance.

(4) The hydrodynamic database used in this study is based on a rigid oscillating cylinder in cross-flow direction. This setup effectively captures the dominant flow mechanisms of VIV in the cross-flow direction at critical Reynolds numbers. As an efficient modeling approach for engineering applications, its simplifying assumptions also define its scope of applicability. It is primarily suitable for operating conditions characterized by a dominant response in the cross-flow direction, weak in-line motion contributions, and structural modal decoupling. Physical phenomena inherent to deep-sea risers, such as two-degree-of-freedom coupling, inline/cross-flow interference, multi-modal interaction, and the fluid-structure feedback of structural flexibility—are currently excluded from the scope of this database model. Future work could focus on systematic expansion to account for factors such as bidirectional coupled response, multimodal excitation mechanisms, inflow turbulence, surface roughness, thereby further enhancing the database's applicability and prediction accuracy under complex operating conditions.

Author Contributions

Conceptualization, H.L. and J.W.; methodology, H.L. and J.W.; software, H.L., Y.G. and Z.T; validation, H.L., Y.G. and J.W.; formal analysis, H.L.; investigation, H.L.; resources, J.W. and Z.T.; data curation, H.L.; writing—original draft preparation, H.L.; writing—review and editing, J.W., Z.T. and Y.C.; visualization, H.L. and Y.G.; supervision, J.W. and Y.C.; project administration, J.W. and Y.C.; funding acquisition, J.W. and Y.C. All authors have read and agreed to the published version of the manuscript.

Funding

This work was supported by the National Natural Science Foundation of China grant number 12172218 and the National Key Research and Development Program of China grant number 2022YFC2806300.

Institutional Review Board Statement

Not applicable.

Informed Consent Statement

Not applicable.

Data Availability Statement

The data that support the findings of this study are available from the corresponding author upon reasonable request.

Conflicts of Interest

The authors declare no conflict of interest.

AI Use Statement

During the preparation of this manuscript, the authors used AI tools solely for language refinement. No AI tools were used for data analysis, interpretation, or generation of scientific content. All outputs were critically reviewed and edited by the authors. The authors take full responsibility for the integrity and accuracy of the work.

Abbreviations

VIV	Vortex-Induced Vibration
LES	Large Eddy Simulation
LSB	Laminar Separation Bubble
CFD	Computational Fluid Dynamics
SGS	Subgrid-Scale
CF	Cross-Flow
IL	In-Line
ELBO	Evidence Lower Bound
BNN	Bayesian Neural Network
DNS	Direct Numerical Simulation
2DOF	Two Degrees of Freedom
HRAPIF	High-Resolution Algorithm Platform for Incompressible Flow
BDAL	Bayesian Deep Active Learning
MAPE	Mean Absolute Percentage Error
RMSE	Root Mean Square Error

Re	Reynolds number	$p(w)$	Prior distribution of network weights
D	Cylinder diameter	$q_\theta(w)$	Variational posterior
U	Inflow velocity	$L(\theta)$	Evidence lower bound (ELBO)
A	Oscillation amplitude	μ_{pred}	Predicted mean
f_e	Oscillation frequency	σ_{ale}	Aleatoric variance
f_s	Vortex shedding frequency	σ_{total}	Total uncertainty
C_{lv}~	Cross-flow excitation coefficient	σ_{epi}	Epistemic uncertainty
C_{my}	Added mass coefficient	$u(z,t)$	Riser horizontal displacement
C_{dm}	Mean drag coefficient	$c(z)$	Hydrodynamic damping coefficient
EI	Flexural rigidity	$m(z)$	Linear density
y^+	Non-dimensional wall distance	$f(z,t)$	Distributed hydrodynamic force
u	Velocity vector	**M**, **C**, **K**	Mass, damping, stiffness matrices
p	Pressure	F	Fluid excitation force vector
ρ	Fluid density	F_y, F_x	Cross-flow/In-line excitation force
ν	Kinematic viscosity	C_{dv}	In-line excitation coefficient
${\tau_{ij}}^{SGS}$	Subgrid-scale stress tensor	$\varphi_k(z)$	k-th mode shape
σ_1, σ_2, σ_3	Eigenvalues of velocity gradient tensor	$Q_k(t)$	k-th modal coordinate
Δ	Filter width	A_k	Modal response amplitude

References

[1] Williamson, C.H.K., Govardhan, R., 2004. Vortex-induced vibrations. Annual Review of Fluid Mechanics. 36, 413–455. DOI: https://doi.org/10.1146/annurev.fluid.36.050802.122128

[2] Sarpkaya, T., 2004. A critical review of the intrinsic nature of vortex-induced vibrations. Journal of Fluids and Structures. 19(4), 389–447. DOI: https://doi.org/10.1016/j.jfluidstructs.2004.02.005

[3] Bearman, P.W., 2011. Circular cylinder wakes and vortex-induced vibrations. Journal of Fluids and Structures. 27(5–6), 648–658. DOI: https://doi.org/10.1016/j.jfluidstructs.2011.03.021

[4] Modarres-Sadeghi, Y., Mukundan, H., Dahl, J.M., et al., 2010. The effect of higher harmonic forces on fatigue life of marine risers. Journal of Sound and Vibration. 329(1), 43–55. DOI: https://doi.org/10.1016/j.jsv.2009.07.024

[5] Feng, C.C., 1968. The measurement of vortex induced effects in flow past stationary and oscillating circular and d-section cylinders [Master's Thesis]. University of British Columbia: Vancouver, BC, Canada.

[6] Khalak, A., Williamson, C.H.K., 1999. Motions, forces and mode transitions in vortex-induced vibrations at low mass-damping. Journal of Fluids and Structures. 13(7–8), 813–851. DOI: https://doi.org/10.1006/jfls.1999.0236

[7] Jauvtis, N., Williamson, C.H.K., 2004. The effect of two degrees of freedom on vortex-induced vibration at low mass and damping. Journal of Fluid Mechanics. 509, 23–62. DOI: https://doi.org/10.1017/S0022112004008778

[8] Jiang, H., Yang, J., Ju, X., et al., 2026. Large-eddy simulation of two-degree-of-freedom vortex-induced vibration of a circular cylinder at Reynolds number 10 000. Journal of Fluid Mechanics. 1035, A20. DOI:

https://doi.org/10.1017/jfm.2026.11545
[9] Guo, P., Zhang, H.F., He, X.H., et al., 2026. Competing vortex shedding modes in vortex-induced vibration dynamics of rectangular cylinders: Geometric dependence of leading/trailing edge synchronization. Ocean Engineering. 351, 124334. DOI: https://doi.org/10.1016/j.oceaneng.2026.124334
[10] Chen, W., Ji, C., Xu, D., et al., 2022. Three-dimensional direct numerical simulations of vortex-induced vibrations of a circular cylinder in proximity to a stationary wall. Physical Review Fluids. 7(4), 044607. DOI: https://doi.org/10.1103/PhysRevFluids.7.044607
[11] Chopra, G., Mittal, S., 2022. Secondary vortex, laminar separation bubble and vortex shedding in flow past a low aspect ratio circular cylinder. Journal of Fluid Mechanics. 930, A12. DOI: https://doi.org/10.1017/jfm.2021.895
[12] Sahu, T.R., Chopra, G., Mittal, S., 2024. Vortex-induced vibration of a circular cylinder in the supercritical regime. Physics of Fluids. 36(10), 105136. DOI: https://doi.org/10.1063/5.0229933
[13] Bishop, R.E.D., Hassan, A.Y., 1964. The lift and drag forces on a circular cylinder oscillating in a flowing fluid. Proceedings of the Royal Society of London. Series A. Mathematical and Physical Sciences. 277(1368), 51–75. DOI: https://doi.org/10.1098/rspa.1964.0005
[14] Morse, T.L., Williamson, C.H.K., 2009. Prediction of vortex-induced vibration response by employing controlled motion. Journal of Fluid Mechanics. 634, 5–39. DOI: https://doi.org/10.1017/S0022112009990516
[15] Sarpkaya, T., 1979. Vortex-induced oscillations: A selective review. Journal of Applied Mechanics. 46(2), 241–258. DOI: https://doi.org/10.1115/1.3424537
[16] Vandiver, J.K., Lee, L., Marcollo, H., et al., 2018. Shear7 v4.10 Theory Manual. Massachusetts Institute of Technology: Cambridge, MA, USA.
[17] Larsen, C., Lie, H., Passano, E., et al., 2017. VIVANA—Theory Manual, Version 4.10.1. SINTEF Ocean: Trondheim, Norway.
[18] Duranay, A., 2024. Numerical and experimental investigation of vortex formation modes on a freely vibrating circular cylinder at high Reynolds numbers. Applied Ocean Research. 144, 103909. DOI: https://doi.org/10.1016/j.apor.2024.103909
[19] Shen, J., Deng, P., Fu, S., et al., 2025. Enhanced vortex-induced vibration prediction of marine risers using excitation coefficient databases at high Reynolds numbers. Journal of Fluids and Structures. 138, 104406. DOI: https://doi.org/10.1016/j.jfluidstructs.2025.104406
[20] Bartran, D., 2025. Strouhal numbers associated with the drag crisis. International Journal of Fluid Engineering. 2(3), 033901. DOI: https://doi.org/10.1063/5.0250747
[21] Zdravkovich, M.M., 1997. Flow around Circular Cylinders, Vol. 1: Fundamentals. Oxford University Press: Oxford, UK.
[22] Achenbach, E., 1968. Distribution of local pressure and skin friction around a circular cylinder in crossflow up to Re = 5 × 106. Journal of Fluid Mechanics. 34(4), 625–639. DOI: https://doi.org/10.1017/S0022112068002120
[23] Schewe, G., 1983. On the force fluctuations acting on a circular cylinder in crossflow from subcritical up to transcritical Reynolds numbers. Journal of Fluid Mechanics. 133, 265–285. DOI: https://doi.org/10.1017/S0022112083001913
[24] Govardhan, R., Williamson, C.H.K., 2000. Modes of vortex formation and frequency response of a freely vibrating cylinder. Journal of Fluid Mechanics. 420, 85–130. DOI: https://doi.org/10.1017/S0022112000001233
[25] Dahl, J.M., Hover, F.S., Triantafyllou, M.S., et al., 2010. Dual resonance in vortex-induced vibrations at subcritical and supercritical Reynolds numbers. Journal of Fluid Mechanics. 643, 395–424. DOI: https://doi.org/10.1017/S0022112009992060
[26] Fan, D., Jodin, G., Consi, T.R., et al., 2019. A robotic Intelligent Towing Tank for learning complex fluid-structure dynamics. Science Robotics. 4(36), eaay5063. DOI: https://doi.org/10.1126/scirobotics.aay5063
[27] Fan, D., Triantafyllou, M.S., 2022. Vortex-induced forces of crossflow and inline oscillating bluff bodies at moderate Reynolds numbers. Marine Structures. 86, 103305. DOI: https://doi.org/10.1016/j.marstruc.2022.103305
[28] Zhao, Z., Wang, J., Shiau, J., et al., 2026. Probabilistic analysis of pile-reinforced slopes considering anisotropic spatial soil properties. International Journal for Numerical and Analytical Methods in Geomechanics. 50(3), 1309–1327. DOI: https://doi.org/10.1002/nag.70125
[29] Zhang, Z., Sun, S., Wang, Z., et al., 2025. Battery retirement state prediction method based on real-world data and the TabNet model. Energy. 334, 137795. DOI: https://doi.org/10.1016/j.energy.2025.137795
[30] Ye, B., Zhang, Z., Wang, S., et al., 2025. State-of-health estimation of lithium-ion battery based on interval capacity for electric buses. IEEE Transactions on Transportation Electrification. 11(2), 6096–6106. DOI: https://doi.org/10.1109/TTE.2024.3497993
[31] Hou, Z., Wang, B., Liu, J., et al., 2025. Physics-inspired time-frequency feature extraction and

lightweight neural network for power quality disturbance classification. Frontiers in Physics. 13, 1616367. DOI: https://doi.org/10.3389/fphy.2025.1616367

[32] Liu, J., Hou, Z., Liu, B., et al., 2025. Mathematical and machine learning innovations for power systems: Predicting transformer oil temperature with beluga whale optimization-based hybrid neural networks. Mathematics. 13(11), 1785. DOI: https://doi.org/10.3390/math13111785

[33] Yin, T., Chen, Y., Wang, Y., et al., 2026. Protein structure prediction powered by artificial intelligence: From biochemical foundations to practical applications. Frontiers in Molecular Biosciences. 13, 1767821. DOI: https://doi.org/10.3389/fmolb.2026.1767821

[34] Hou, Z., Liu, J., Pang, J., 2025. Green transition and climate adaptation: Empirical evidence of corporate resilience in the low-carbon economy. Global NEST Journal. 27(6), 1–22. DOI: https://doi.org/10.30955/gnj.07421

[35] Ren, H., Fu, S., Zhang, M., et al., 2024. Mapping vortex-induced forces of oscillating bluff bodies from subcritical to critical Reynolds numbers. Physical Review Fluids. 9(9), L092701. DOI: https://doi.org/10.1103/PhysRevFluids.9.L092701

[36] Gong, Y., Wang, J., 2024. Turbulence model adaptability at critical Reynolds numbers and applications in wake control via fairings. Applied Ocean Research. 153, 104263. DOI: https://doi.org/10.1016/j.apor.2024.104263

[37] Ding, Z.J., Balasubramanian, S., Lokken, R.T., et al., 2004. Lift and damping characteristics of bare and straked cylinders at riser scale Reynolds numbers. In Proceedings of the Offshore Technology Conference, Houston, TX, USA, 3–6 May 2004. DOI: https://doi.org/10.4043/16341-MS

[38] Gopalkrishnan, R., 1993. Vortex-induced forces on oscillating bluff cylinders [PhD Thesis]. Massachusetts Institute of Technology: Cambridge, MA, USA.

[39] Soni, P.K., 2008. Hydrodynamic coefficients for vortex-induced vibrations of flexible beams [PhD Thesis]. Norwegian University of Science and Technology: Trondheim, Norway.

[40] Chaplin, J.R., Bearman, P.W., Huera Huarte, F.J., et al., 2005. Laboratory measurements of vortex-induced vibrations of a vertical tension riser in a stepped current. Journal of Fluids and Structures. 21(1), 3–24. DOI: https://doi.org/10.1016/j.jfluidstructs.2005.04.010

[41] Chaplin, J.R., Bearman, P.W., Cheng, Y., et al., 2005. Blind predictions of laboratory measurements of vortex-induced vibrations of a tension riser. Journal of Fluids and Structures. 21(1), 25–40. DOI: https://doi.org/10.1016/j.jfluidstructs.2005.05.016

[42] Huera-Huarte, F.J., 2006. Multi-mode vortex-induced vibrations of a flexible circular cylinder [PhD Thesis]. Imperial College London: London, UK.

[43] Gong, Y., Zheng, H., Xu, H., et al., 2026. Numerical simulation of vortex-induced vibration of a full-scale flexible riser at supercritical Reynolds number in uniform and linear shear flow. Ocean Engineering. 352(1), 124414. DOI: https://doi.org/10.1016/j.oceaneng.2026.124414

[44] Gong, Y., 2026. Numerical simulation of vortex-induced vibration of marine risers at critical Reynolds numbers and its suppression [PhD Thesis]. Shanghai Jiao Tong University: Shanghai, China. (in Chinese)

[45] Jia, X., Jia, L., Huang, J., et al., 2021. Research on overall design of steel catenary riser for “Deep Sea No. 1” energy station. China Offshore Oil and Gas. 33(5), 165–174.